ECOHYDROLOGY
Ecohydrol. **3**, 189–204 (2010)
Published online 19 May 2010 in Wiley InterScience
(www.interscience.wiley.com) DOI: 10.1002/eco.129

Topographical and ecohydrological controls on land surface temperature in an alpine catchment

G. Bertoldi,[1]* C. Notarnicola,[2] G. Leitinger,[1,3] S. Endrizzi,[4] M. Zebisch,[2] S. Della Chiesa[1,3] and U. Tappeiner[1,3]

[1] *Institute for Alpine Environment, EURAC Research, Bolzano, Italy*
[2] *Institute for Applied Remote Sensing, EURAC Research, Bolzano, Italy*
[3] *Institute of Ecology, University of Innsbruck, Innsbruck, Austria*
[4] *National Hydrology Research Centre—Environment Canada, Saskatoon, Canada*

ABSTRACT

In mountain areas, land surface temperature (LST) is a key parameter in the surface energy budget and is controlled by a complex interplay of topography, incoming radiation and atmospheric processes, as well as soil moisture distribution, different land covers and vegetation types. In this contribution, the LST spatial distribution of the Stubai Valley in the Austrian Alps is simulated by the ecohydrological model GEOtop. This simulation is compared with ground observations and a Landsat image in order to assess the capacity of the model to represent land surface interactions in complex terrain, as well as to evaluate the relative importance of different environmental factors. The model describes the energy and mass exchanges between soil, vegetation and atmosphere. It takes account of land cover, soil moisture and the implications of topography on air temperature and solar radiation. The GEOtop model is able to reproduce the spatial patterns of the LST distribution estimated from remote sensing, with a correlation coefficient of 0·88 and minimal calibration of the model parameters. Results show that, for the humid climate considered in this study, the major factors controlling LST spatial distribution are incoming solar radiation and land cover variability. Along mountain ridges and south-exposed steep slopes, soil moisture distribution has only a minor effect on LST. North- and south-facing slopes reveal a distinct thermal behaviour. In fact, LST appears to follow the air temperature vertical gradient along north-facing slopes, while along south-facing slopes, the LST vertical gradient is strongly modified by land cover type. Both Landsat observations and model simulations confirm field evidence of strong warming of alpine low vegetation during sunny days and indicate that these effects have an impact at a regional scale. Our results indicate that in order to simulate LST in mountain environments using a spatially distributed hydrological model, a key factor is the capacity to explicitly simulate the effects of complex topography on the surface energy exchange processes. Copyright © 2010 John Wiley & Sons, Ltd.

KEY WORDS surface temperature; remote sensing; alpine ecology; hydrological models

Received 1 July 2009; Accepted 7 March 2010

INTRODUCTION

Accurate modelling of the surface energy and water budget is needed to predict the effects of climate and land use changes on water resources, vegetation and ecosystems. While significant progress has been made in estimating the surface budget components (i.e. surface temperature, sensible and latent heat fluxes) at the global and regional scale (Lawford *et al*., 2004), further efforts are needed to improve spatial accuracy and modelling capabilities in mountain regions (Brooks and Vivoni, 2008). In fact, mountain regions present extreme variability, often being characterized by steep slopes and altitude variations of thousands of metres. The complex structure of the landscape is also reflected in patched land cover and vertically structured ecosystems (Becker *et al*., 2007).

Spatially distributed hydrological and land surface models (e.g. Wigmosta *et al*., 1994; Ivanov *et al*., 2004; Kunstmann and Stadler, 2005) are able to describe land surface interactions in complex terrain, both in the temporal and spatial domains. However, they require high-quality and spatially resolved observations in order to be validated (Grayson and Blöschl, 2000; Schulz *et al*., 2006). Land surface temperature (LST) is a key parameter in the surface energy budget as well as water budget, through evapotranspiration (Diak *et al*., 2004). Since LST is easily available through remote sensing (Turner *et al*., 2001), it can be used to validate and improve distributed land surface models (Wang *et al*., 2009).

Currently available satellite thermal infrared sensors provide data with different spatial resolution that can be used to estimate LST. The Geostationary Operational Environmental Satellite has a 4-km resolution in thermal infrared, while the National Oceanic and Atmospheric Administration (NOAA)-Advanced Very High-Resolution Radiometer and the Terra and Aqua-Moderate Resolution Imaging Spectroradiometer have 1-km spatial resolutions (Wang *et al*., 2009). However, in mountain landscapes, due to the complex topography, high-resolution data are needed. The Terra-Advanced Spaceborne Thermal Emission and Reflection

* Correspondence to: G. Bertoldi, Institute for Alpine Environment, EURAC Research, Viale Druso 1, I-39100 Bolzano, Italy. E-mail: giacomo.bertoldi@eurac.edu

Radiometer, which has a 90-m pixel resolution, and the Landsat-7 Enhanced Thematic Mapper (ETM), which has a 60-m resolution, both contain the high-resolution data required (Li *et al.*, 2004). In this paper, Landsat-7 data have been considered because they have the highest spatial resolution.

In mountain landscapes, the LST spatial distribution is connected with the topography through the interplay of different factors:

1. Elevation, slope and aspect exert a direct control on the incoming solar radiation (Dubayah *et al.*, 1990). At the same time, elevation and the atmospheric boundary layer of the valley affect the air temperature, moisture and wind distribution (e.g. Rampanelli, 2004; Garen and Marks, 2005; Chow *et al.*, 2006).
2. Vegetation is organized along altitudinal gradients, and canopy structural properties influence turbulent heat transfer processes, radiation divergence (Wohlfahrt *et al.*, 2003) and transpiration, and therefore LST. While forests tend to have a canopy temperature closer to air temperature (Körner, 2007), prostrate high-altitude vegetation tends to create its own microclimate decoupled from atmospheric conditions, with a strong temperature increase in sunny conditions (Körner, 2003). At higher altitude, very steep slopes, rocky surfaces and patchy snow cover strongly influence LST.
3. Soil moisture influences sensible and latent heat partitioning and therefore LST. Topography controls the catchment-scale soil moisture distribution (Beven and Freer, 2001) in combination with soil properties (Romano and Palladino, 2002), soil thickness (Heimsath *et al.*, 1997) and vegetation (Brooks and Vivoni, 2008).

In this paper, we compare the LST distribution simulated by the ecohydrological model GEOtop (Rigon *et al.*, 2006) with a Landsat thermal image and ground observations for an alpine catchment. This comparison aims to improve the process description and parameter identification of the model as well as to evaluate the relative importance of the different environmental factors.

The GEOtop model describes the soil–vegetation–atmosphere energy and mass exchanges, taking into account the impact of elevation on air temperature, the effects of slope and exposure/position on solar radiation as well as the spatial distribution of vegetation and water content. Since the model calculates LST as a result of the surface energy budget, a correct LST estimation is a good indication of a correct description of model processes.

The model is considered here as a tool for understanding of processes. In order to identify which processes are most relevant (i.e. the level of complexity required for the model) for capturing the main spatial patterns of LST, simulations with different model configurations were performed:

1. with uniform or spatially variable land cover properties, in order to separate the effect of incoming solar radiation from land cover properties on LST distribution and
2. with uniformly humid or spatially distributed soil moisture conditions, to quantify the role of soil moisture distribution on LST, because it is linked with the energy partitioning in sensible and latent heat fluxes.

The first part of the paper presents a description of the study area, the currently available remote sensing and ground observations, the GEOtop model structure and the simulation parameterizations. This is followed by a point-scale comparison of Landsat and simulated LST with ground observations and by a spatial comparison of the observed–simulated LST patterns. Finally, the capacity of the model to simulate LST and the relative importance of the different controlling factors are discussed.

STUDY REGION, REMOTE SENSING AND GROUND OBSERVATIONS

Study region

The study region is a 257-km^2 area of the Stubai Valley, located southwest of the city of Innsbruck in the Austrian Alps. This region has been chosen because it is representative of a high-alpine environment and because of the good availability of data (Tenhunen *et al.*, 2009).

The altitude extends from 900 m a.s.l. in the northern valley floor to 3450 m a.s.l. at the southern end of the valley (Figure 1a), and the climate is humid and classified as temperate continental inner-alpine. It is characterized by wet summers, with frequent precipitation and heavy thunderstorms. About 50% of the annual precipitation falls as snow during the winter. The average annual air temperature is 6·3 °C and the annual precipitation is 850 mm at valley sites and about 3·0 °C and 1100 mm at the treeline (near to 1900 m). Less than 1% of the study region is urbanized, 8% of the surface is covered by glaciers, 31% is rock cover, 23% is natural or abandoned grasslands, 9% is managed grasslands and the remaining 27% is forest (Tappeiner *et al.*, 2008).

Forests are dominated by dense formations of Norway spruce (*Picea abies*) and by more open stands of *Larix decidua*, prevalent at both the treeline and on south-facing slopes. Deciduous forest groves of *Salix* sp., *Alnus viridis* and *Sorbus aucuparia* are locally significant. Grasslands differ in management intensity and include intensively used meadows, located mostly at the bottom of the valley. These meadows are heavily fertilized and cut two to three times a year (*Trisetetum flavescentis* community). At a higher altitude, lightly used meadows are found, particularly on south-facing slopes. These are less heavily fertilized and cut once a year (Sieversio-*Nardetum strictae* community). At and above the treeline are managed pastures (*Seslerio-Caricetum* community) as well as abandoned pastures and meadows, which are undergoing succession with the invasion of shrubs and tree seedlings. Natural alpine grassland occurs at locations above the managed grasslands, and above

DOI: 10.1002/eco

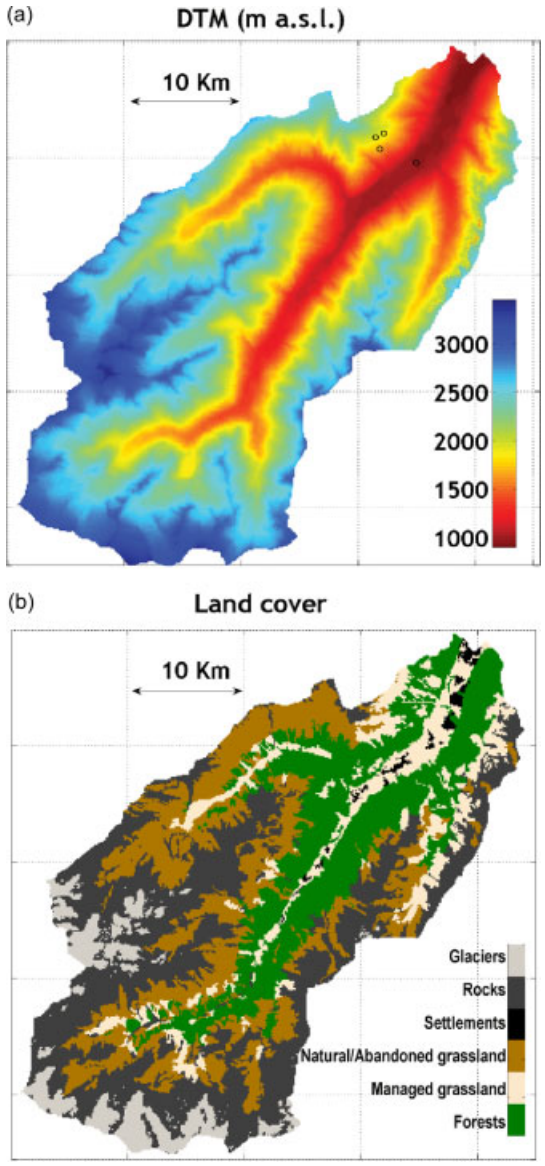

Figure 1. The study area of Stubai Valley, located in the Central Alps in Tyrol, Austria. Above: digital terrain model (DTM). The black circles indicate the location of the meteorological stations considered in this study. Below: the main land cover types from Tappeiner *et al.* (2008), modified.

2700 m a.s.l. rocks and glaciers is the dominant land cover.

Remote sensing data

In this paper, one Landsat ETM plus image acquired on 13 September 1999 at 10·50 am was considered. The weather conditions were typical of a clear late summer day in this area. According to records of the meteorological stations of Telves and Krossbach of the Hydrographic Service of the Tiroler Landesregierung, there was no rainfall in the area in the previous 5 days. However, in the previous month, the total precipitation was between 100 and 80 mm, a value comparable with the climatic mean precipitation for this time of year.

The Landsat image was used to produce an LST map with 60-m resolution by using the band 6, which covers the wavelength from 10·4 to 12·5 μm. Having one single thermal band, the Landsat data have been rarely used to determine the LST because of the difficulty of correcting them adequately for the atmospheric effects. These corrections require an accurate radiative transfer model and knowledge of the atmospheric aerosols' profile and surface emissivity (Qin *et al.*, 2001). In this case, since atmospheric soundings were not available, the standard approach of Thome *et al.* (2000) was followed, by transforming the radiance in brightness temperature and validating the output temperature values with ground measurements of specific targets (Table I).

The surface emissivity was considered constant and equal to 1. This assumption may create major discrepancies, especially for bare soil, since in this case, soil emissivity can vary significantly in the wavelength range from 10·4 to 12·5 μm, while vegetation canopies have high effective emissivities at all wavelengths. However, in the chosen study region, the area covered by bare soil is relatively small (<1%), and the focus of this paper is alpine vegetation.

Ground observations

The quality of remote sensing and modelled LST was assessed through micrometeorological observations,

Table I. Land cover, topographical properties and temperature observations on 13 September 1999 at 11 am used to estimate T_a at the upper elevations.

Land use	Stations				
	PA1900	AB1900	LM1700	M970	S3330
	Moderately managed grassland	Abandoned grassland	Larch meadow	Intensively managed grassland	Rock
Elevation (m a.s.l.)	1908	1938	1696	975	3330
Aspect, from E, counter hourly	327	294	305	—	—
Inclination (°)	26	27	22	1	—
T_a (°C)	17	18.6	21.5	19.8	6.6
T_c (°C)	20.4	19.8	22.8	20.7	—
T_{ac} (°C)	24.2	21.5	23.7	23	—

The stations observed were: stations PA1900, AB1900 and LM1700, situated in the area of Kaserstattalm along the southeastern slope; station M970 in the valley bottom close to Neustift in Stubaital and station S3330, situated on Schöntauferspitze near Sulden, about 70 km south of the study region. The air temperature T_a was measured 2 m above the ground; T_{ac} is the leaf temperature inside the canopy and T_c is the leaf temperature at the top of the canopy.

DOI: 10.1002/eco

which were collected within the framework of the ECOMONT project (Cernusca *et al.*, 1999). Four meteorological stations with different elevation and land use were available inside the study area (Figure 1), as indicated in Table I:

- Station M970 in an intensively managed meadow on the floor of the valley at 970 m.
- Station LM1700 in a *L. decidua* southeast-exposed meadow at 1700 m.
- Station AB1900 in a southeast-exposed abandoned pasture at 1900 m.
- Station PA1900 in a southeast-exposed moderately used pasture at 1900 m.

In order to estimate air temperature at upper elevations, the data from Schöntauferspitze (Station S3300), located at 3330 m, about 70 km southwest of Stubai, have been considered. Because of its altitude, data from this station represent free atmospheric conditions, which show little spatial variability, because at that elevation the atmosphere is little affected by the atmospheric boundary-layer processes occurring in the valley (Weigel *et al.*, 2007).

For each experimental site, measurements of air (T_a) and leaf temperatures within and at the top of the canopy (T_{ac} and T_c, respectively) were taken with small thermocouples. As all sites were covered by a dense canopy [leaf area index (LAI) >4], T_c can be considered as representative of effective LST. The observed T_a, T_{ac} and T_c at the time of the Landsat overpass are reported in Table I. In all grassland sites, the vegetation is warmer than the air, from sunrise throughout the day, as observed in a similar environment by Cernusca and Seeber (1989a,b).

METHODS AND SIMULATION PARAMETERIZATIONS

In this section, a brief description of the model, simulations, parameterizations and approaches used to analyse the results are reported.

The model GEOtop

GEOtop is a fully spatially distributed process-based hydrologic model. In this paper, only a brief overview of the model's capabilities is presented. An overall description can be found in Rigon *et al.* (2006), Zanotti *et al.* (2004) and Endrizzi (2009). The GEOtop model displayed good ability in reproducing the pointwise and catchment-scale energy and water balance in different mountain catchments (e.g. Bertoldi *et al.*, 2006; Simoni *et al.*, 2007).

The model is able to simulate the following processes: (i) coupled soil vertical water and energy budgets, through the resolution of the heat and Richard's equations, with temperature and water pressure as prognostic variables, (ii) surface energy balance in complex topography, including shadows, shortwave and longwave radiation, turbulent fluxes of sensible and latent heat, as well as considering the effects of vegetation as a boundary condition of the heat equation, (iii) ponding, infiltration, exfiltration and root water extraction as a boundary condition of Richard's equation, (iv) subsurface lateral flow, solved explicitly and considered as a source/sink term of the vertical Richard's equation, (v) surface runoff by kinematic wave and (vi) multilayer glacier and snow cover, with a solution of snow water and energy balance fully integrated with soil.

The incoming direct shortwave radiation is computed for each grid cell according to the local solar incidence angle θ, including shadowing (Iqbal, 1983). It is also split into a direct and diffuse component according to atmospheric and cloud transmissivity (Erbs *et al.*, 1982). The diffuse incoming shortwave and longwave radiation is adjusted according to the fraction of sky visible from each point, in order to account for the local screening by the surrounding mountains (Dubayah *et al.*, 1990).

The soil column is discretized in several layers of different thicknesses. The most superficial layer is normally set at a very low degree of thickness (around 10 mm) so that its temperature and water pressure can be considered as representative of the surface conditions. The heat and Richard's equations are written, respectively, as

$$C_t(P)\frac{\partial T}{\partial t} - \frac{\partial}{\partial z}\left[K_t(P)\frac{\partial T}{\partial z}\right] = 0 \quad (1)$$

$$C_h(P)\frac{\partial P}{\partial t} - \frac{\partial}{\partial z}\left[K_h(P)\left(\frac{\partial P}{\partial z} + 1\right)\right] - q_s = 0 \quad (2)$$

where T is the soil temperature, P the water pressure, C_t the thermal capacity, K_t the thermal conductivity, C_h the specific volumetric storativity, K_h the hydraulic conductivity and q_s the source term associated with lateral flow. The variables C_t, K_t, C_h and K_h depend on water content, and, in turn, on water pressure, and are therefore a source of non-linearity. The boundary conditions at the surface are consistent with the infiltration and surface energy balance and are given in terms of surface fluxes of water (Q_h) and heat (Q_t) at the surface, namely

$$Q_h = \min\left(p_{net}, K_{h1}\frac{(h - P_1)}{dz/2} + K_{h1}\right) - E(T_1, P_1) \quad (3)$$

$$Q_t = SW_{in} - SW_{out} + LW_{in} - LW_{out}(T_1) - H(T_1) - LE(T_1) \quad (4)$$

where p_{net} is the net precipitation, K_{h1} and P_1 the hydraulic conductivity and water pressure of the first layer, h the pressure of ponding water, dz the thickness of the first layer and T_1 the temperature of the first layer (which is an approximation of LST, i.e. Best, 1998). E is evapotranspiration (as water flux), SW_{in} and SW_{out} the incoming and outgoing shortwave radiation, LW_{in} and LW_{out} the incoming and outgoing longwave radiation, H the sensible heat flux and LE the latent heat flux. H and

DOI: 10.1002/eco

LE are calculated taking into consideration the effects of atmospheric stability (Monin and Obukhov, 1954). E is partitioned by soil evaporation and transpiration, depending on the soil and canopy resistances (Dickinson *et al*., 1991). At the bottom of the soil column, a boundary condition of zero fluxes has been imposed.

In the surface energy balance calculation, fluxes are calculated for unit surface area (W m^{-2}). The area of pixels is considered taking into account their slope. Therefore, the surface energy fluxes that are not dependent on gravity are considered normal to the surface (Pomeroy *et al*., 2003) and are then referred to the unit of their actual area. As a result, no cosine correction is needed, except for the fluxes that depend on gravity, such as vertical water flows, which, conversely, are cosine corrected. This means that the calculation of LST is not affected by the different exchange areas of a flat cell compared with an inclined one.

Each grid cell has the same resolution of the Landsat data, and it is partitioned into a vegetated and bare soil (or rock) fraction. The model calculates an effective LST as weighted balance of soil and vegetation contributions (Norman *et al*., 1995).

For details of the numerical implementation, see Endrizzi (2009). The code of the model is open source and can be downloaded from the following Web site: http://www.geotop.org/.

Simulation parameterizations

The model requires meteorological data collected in one or more ground stations, i.e. air temperature (T_a), air specific humidity (q_a), precipitation (P), wind speed (U) and solar shortwave radiation (R_{sw}). Meteorological data from Neustift (station M970 in Table I) have been used as model input. Air temperature T_a for each grid cell was adjusted with respect to elevation, assuming a standard air temperature lapse rate γ of -6 K km^{-1} (Garen and Marks, 2005), as discussed later in the text. Precipitation was measured at the stations of Telves and Krossbach belonging to the Hydrographic Service of the Tiroler Landesregierung and spatially interpolated using ordinary kriging (Kitanidis, 1997).

Topographical properties such as slope, aspect and surface curvature were derived from a 20-m grid resolution digital elevation model (DEM) of the catchment, obtained by the Federal Government of Tyrol (TIRIS—Tiroler Informations System). All the map inputs of the model were then resampled at 60 m, to match Landsat grid resolution. Soil hydraulic properties were calculated as in Vereecken *et al*. (1989), considering soil samples collected in the proximity of the Neustift station. Since detailed soil data in the whole basin are lacking, the same soil profile was assumed. However, the soil thickness was calculated inverting the soil production model of Heimsath *et al*. (1997), which relates the soil thickness to the local curvature, assuming a stationary balance between soil production and erosion as well as considering soil production as a diffusive process. This model can be further developed to obtain an expression for soil thickness as a function of the local curvature (which has been derived from the DEM) as explained in Bertoldi *et al*. (2006). With this model, the soil thickness in convex areas of the catchment decreases up to a critical curvature value that corresponds to bare rock outcrops. For the convex areas, a constant soil thickness of 0·5 m has been assumed. Land cover was procured from an accurate map of the Stubai Valley developed by Tappeiner *et al*. (2008) from aerial photographs, historical maps and field surveys, using the methodology explained in Tasser *et al*. (2009). The original map at 20-m grid resolution was then resampled at 60 m.

The main model parameters relevant to LST calculation for the different land covers are reported in Table II. Soil surface and vegetation properties such as albedo (a), aerodynamic surface roughness (z_0), displacement height (d_0), LAI and rooting depth (d_r) have been assigned for each land cover class from the literature values (Findell *et al*., 2007) and validated by field surveys (Hammerle *et al*., 2008). Parameters for grasslands have been derived from the studies of Cernusca and Seeber (1989a,b), who analysed a south-facing transect in the Austrian Alps, which included a hay meadow at 1600 m a.s.l., a pasture at 1900 m a.s.l. and an alpine grassland of the Seslerietum–Curvuletum type at 2300 m a.s.l. These habitats can also be considered as representative

Table II. Parameters used in the model for the considered land cover classes.

Model parameters	Land use classes							
	Forests	Intensively managed grassland	Moderately managed grassland	Lightly managed grassland	Abandoned grassland	Natural grassland	Rocks	Glaciers
f_c (−)	1	1	1	1	1	0·5	0	0
d_r (m)	0·5	0·15	0·15	0·15	0·20	0·20	0	0
a (−)	0·2	0·2	0·2	0·2	0·15	0·15	0·15	0·7
z_0 (m)	1	0·04	0·02	0·02	0·01	0·01	0·01	0·01
d_0 (m)	6·6	0·264	0·132	0·132	0·066	0·066	0·0	0·0
LAI (−)	7·0	6·0	5·0	4·0	3·0	1·0	—	—

In the presentation of results, the three classes of managed grasslands have been grouped into a single class 'managed grasslands' and the two classes 'abandoned grassland' and 'natural grassland' have been grouped into the class 'natural abandoned grasslands'. f_c, fraction of the soil covered by canopy; d_r, rooting depth (m); a, albedo (−); z_0, surface roughness (m); d_0, displacement height (m); LAI, leaf area index (−).

DOI: 10.1002/eco

of the Stubai Valley. Cernusca and Seeber (1989b) found a decrease in altitude of LAI (from 7 to 2) and canopy height (h_c; from 90 to 12 cm) and a displacement height (d_0) of about 0·45 h_c. LAI can also be deduced from the Landsat image. However, we did not use input information based on the Landsat image in the model. This was done in order to have a cleaner comparison between satellite- and model-estimated LST maps.

In order to reach a dynamic equilibrium for LST and surface soil moisture, the model was run during the whole of 1999. The hourly average from 10 am up to 11 am of the modelled LST for 13 September was used as a comparison with the Landsat image, considering the same grid resolution (60 m). This simulation, with spatial soil moisture and land cover variation, has been considered as reference simulation ('base' simulation).

Effects of land cover parameterization on LST estimation

A sensitivity analysis was conducted in order to identify the most relevant parameters that characterize the thermal behaviour of different land covers. A series of plot-scale simulations, with the same meteorological forcing but different land cover, were conducted. The parameters that turned out to have the maximum effect on LST predictions were z_0, albedo and LAI.

In GEOtop, the parameter z_0 strongly influences land cover surface temperature. An increase in z_0 implies a stronger turbulent heat exchange between surface and atmosphere, with a decrease in LST during the day. This is confirmed by the Landsat image, which shows lower LST for the south-exposed forested areas (with high z_0) compared with grasslands. Albedo has a significant impact on LST. However, since no detailed information on the albedo of the different land covers was available, it has been kept spatially constant across the catchment. LAI has a relevant impact on canopy transpiration, but exerts a minor effect on LST, as long as transpiration is not water limited, as is generally the case for humid climates. All other biophysical parameters reported in Table II (root and stomatal properties) change only slightly between grassland and forest for snow-free periods (Findell *et al*., 2007), and they did not reveal a significant impact on the modelled LST.

Analyses of model results and simulation scenarios

Here, we provide a brief overview of the approaches used to evaluate and analyse model results. First, the Landsat-retrieved LST (in the following indicated as LST_L) and the corresponding GEOtop-simulated LST (indicated as LST_G) are compared against ground observations (Comparison with Ground Observations Section). Second, the LST_L and LST_G spatial distributions are compared with each other (Landsat and GEOtop LST Comparison Section). Third, an explorative statistical analysis based on ordinary least-squares (OLS) regression was used to show the relative contribution of 'Sun incidence angle', 'elevation', 'land cover' and 'soil moisture' on LST_L and LST_G (OLS Regression Results—Determinants of LST Section). Finally, the physical role of each factor in determining the observed LST patterns is discussed with the aid of a set of simulations with different model configurations (Sun Incidence Angle, Elevation, Land Cover, The Effects of Alpine Vegetation on LST Distribution and Role of Soil Moisture Spatial Variability Sections).

The simulation 'base' takes into account the spatial variability of all factors. In order to consider the role of soil moisture distribution alone LST, a second simulation was performed assuming uniformly saturated soil over the whole catchment at the time of the Landsat overpass ('wet' simulation). A third simulation with both uniform soil moisture and land cover properties (grassland) was also performed ('uniform' simulation). The comparison of this simulation with the 'base' simulation highlights the effect of spatial variability of land cover properties from other topographical factors controlling LST distribution.

OLS regression approach

An OLS regression with the independent variables 'Sinus of Sun incidence angle', 'elevation Z', 'land cover' and 'soil moisture' was conducted. The resulting model reveals the significant factors influencing LST as well as the relative contribution of each independent variable. The variable 'Sinus of Sun incidence angle' is calculated as the Sinus of Sun incidence angle $\Phi = \sin(\theta)$ at the time of the Landsat overpass, and it is considered here as a proxy of the effect of aspect on solar radiation. $\Phi < 0$ indicates sun along the local horizon, and pixels with low Φ values will be mainly north exposed, while $\Phi < 1$ indicates sun at the local zenith. The variable 'elevation Z' can also be considered as a proxy of the air temperature lapse rate. The variable 'land cover' was split into dummy variables for each land cover type, in order to meet the requirements for OLS regression. As distributed soil moisture observations were not available in the catchment, the variable 'soil moisture' represents the volumetric soil water content simulated by the model in the first 5 cm of soil.

The resulting standardized coefficients reflect the influential power of the independent variable in the regression model, while the sign describes a positive or negative correlation with the dependent variable. The resulting part correlation is the correlation between the dependent variable and an independent variable, when the linear effects of the other independent variables in the model have been removed from the independent variable. In other words, the ratio of the part correlation between two variables is directly related to its relative influence on LST. Results of the OLS regression are discussed in OLS Regression Results—Determinants of LST Section.

RESULTS AND DISCUSSION

Comparison with ground observations

The quality of remote sensing and modelled LST is compared here against the available ground observations.

DOI: 10.1002/eco

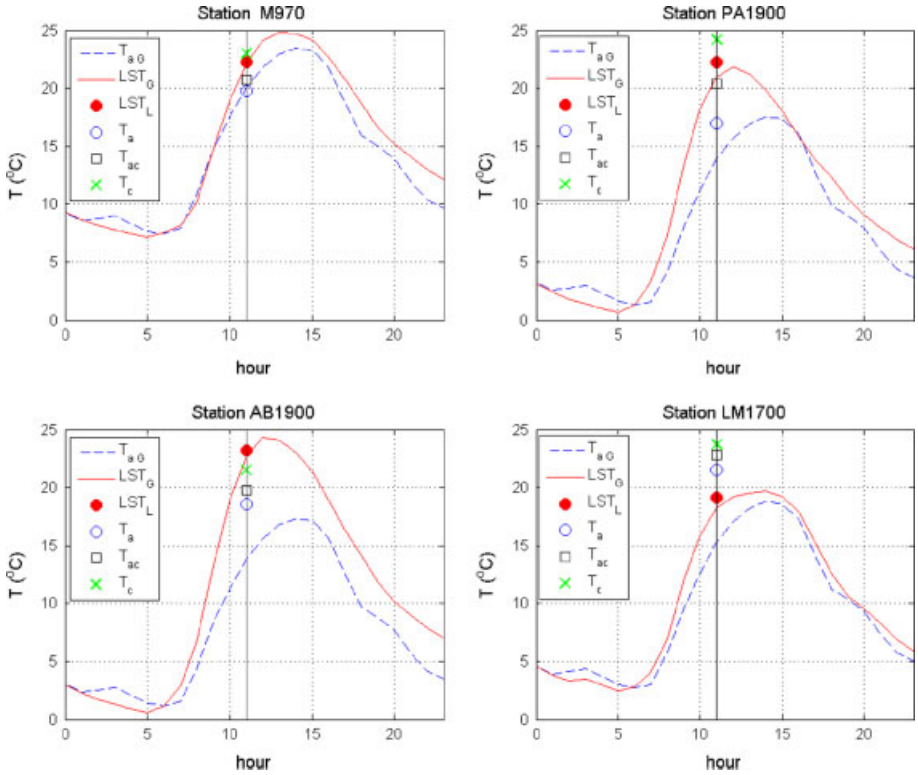

Figure 2. The modelled diurnal cycle for 13 September 1999 of LST_G is compared with LST_L as well as the observed canopy and air surface temperatures for the locations where ground observations were available (Table I). LST_G, GEOtop-estimated LST for the 'base' simulation; T_{aG}, GEOtop-estimated air temperature for the pixels corresponding to the stations; LST_L, Landsat-retrieved LST; T_a, air temperature observed 2 m above the ground; T_{ac}, leaf temperature inside the canopy; T_c, leaf temperature at the top of the canopy.

Figure 2 reports the observed surface canopy temperatures T_c for the four stations inside the simulation domain, the Landsat estimated LST_L and the daily cycles of the GEOtop-simulated air (T_{aG}) and surface (LST_G) temperatures for the pixel corresponding to the stations. The simulated LST_G matches well with LST_L in all four different locations. The differences of LST_L with the observed T_c are within the 2 K accuracy level of the Landsat-retrieved temperature (Thome *et al.*, 2000).

Both Landsat and GEOtop underestimate T_c for the station LM1700. The error can be related to the coarse pixel resolution. In fact, this station is located in a grassy patch inside a sparse Larch forest. While the station is representative of the meadow, the corresponding Landsat and GEOtop pixels are also sampling the surrounding trees. Forests have a higher surface roughness compared with grasslands, and this implies a stronger turbulent exchange at the top of the canopy (McNaughton and Jarvis, 1991; Larcher, 2003) leading to lower top canopy temperatures, which are closer to air temperature (Wilson *et al.*, 1987; Grace *et al.*, 1989; Körner and Paulsen, 2004).

The model underestimates the observed T_a in all locations, except station M970. This occurs because the model was forced by an imposed γ of -6 K km^{-1}, while the gradient between the M970 and PA1900 stations is only $-2{\cdot}7$ K km^{-1}. In fact, stations AB1900, PA1900 and LM1700 are on a southeast-facing slope, and they experience an earlier warming because they receive more morning solar radiation than station M970, which is in the valley bottom. During late morning hours, a residual atmospheric boundary layer in the valley may be present (Stull, 1988). However, the observed T_a gradient between the lowest station (M970) and the highest station (S3330) is about $-5{\cdot}5$ K km^{-1}, supporting the choice of assuming a standard climatic value $\gamma = -6$ K km^{-1} in the model.

The fact that the model matches LST_L relatively well even when forced by a locally biased T_a value is a strong indication that the model correctly reproduces the local surface energy budget and that the energy forcing plays a more important role in controlling LST with respect to T_a.

Landsat and GEOtop LST comparison

In Figure 3, LST_L and the corresponding LST_G maps are compared. The model is able to reproduce the main patterns well, with a spatial correlation coefficient $\rho(LST_L, LST_G) = 0{\cdot}88$, a root mean square error $RMSE(LST_L, LST_G) = 4{\cdot}3$ K and an overall bias $< LST_G — LST_L > = -2{\cdot}1$ K, as reported in Table III. The Landsat image shows large LST variations, related to mountain topography and land cover. Glaciated or snow-covered areas have $LST_L \approx 0$ K, sun-facing slopes covered by a mixture of rocks and natural grasslands show high LST_L values, and managed meadows in the valley have higher LST_L values than forests along the side slopes.

The differences between LST_G and LST_L and the RMSE for the main land cover classes are illustrated in Figure 4. The model captures the observed LST well for snow-covered or glaciated areas (Figure 4a). Forests

DOI: 10.1002/eco

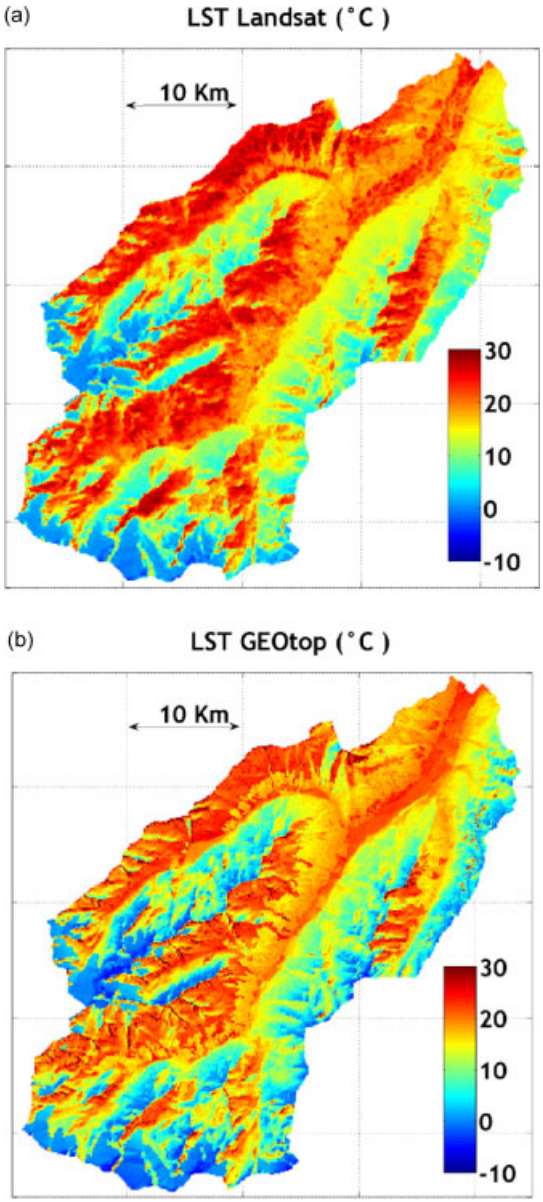

Figure 3. Above: Landsat-retrieved LST (LST_L) on 13 September 1999 at 10·50 am; below: GEOtop-simulated LST (LST_G) for the same hour and day (simulation 'base').

(Figure 4a) and grassland classes (Figure 4b and c) also exhibit good accordance. When vegetation is dense, LST shows less local variations. Results show a significant scatter for rocky slopes (Figure 4d), where LST is related to the local exposure and surface properties, revealing a fine-scale spatial variability not captured at the 60-m grid resolution considered in this research.

We addressed the resolution problem by analysing the land cover map at its original resolution (20 m) and then testing model predictions only for the 60-m 'clean' grid cells that have uniform land cover. However, there is almost no improvement in the model's predictions using 'clean' grid cells. In fact, the RMSE(LST_L, LST_G) considered only the clean cell changes from 4·3 to 4·2 K. This means that, particularly in rocky areas, the scale of variability is below the 20-m resolution of the land cover map. For example, in a 20 m × 20 m pixel, it can be a mix of rocky and grassy patches. A mixed land cover can be included in the model by considering a fractional canopy fraction. However, a test with the model, assuming a canopy fraction of 0·5 for the class 'natural/abandoned grasslands' and of 0·2 for the class 'rocks', showed only slight differences in the LST patterns. The overall spatial correlation changed only from 0·876 to 0·873.

Table III. Statistics of the considered fields.

	Simulation base	Simulation uniform	Simulation wet
$< LST_L — LST_G >$	−2·13	−3·13	−2·76
$\sigma(LST_L — LST_G)$	3·69	4·81	3·25
$\rho(LST_L, LST_G)$	0·88	0·74	0·88
$RMSE(LST_L, LST_G)$	4·26	5·74	4·27
$\rho(LST_L, \Phi)$	0·68	0·68	0·68
$\rho(LST_G, \Phi)$	0·76	0·83	0·75
$\rho(LST_L, Z)$	−0·35	−0·35	−0·35
$\rho(LST_G, Z)$	−0·38	−0·51	−0·51

$<x - y>$ is the difference in the averages in K, $\sigma(x - y)$ is the standard deviation of the differences, $\rho(x, y)$ is the correlation coefficient, RMSE(x, y) is the root mean square error in K, LST_L the Landsat-retrieved LST, LST_G is the GEOtop-simulated LST, $\Phi = \sin(\theta)$, where θ is the Sun incidence angle at the time of the Landsat overpass and Z is the cell elevation (m).

LST_L—LST_G differences tend to increase with elevation, as shown in Figure 5. The strongest model underestimation is for the elevation rank between 2000 and 2500 m a.s.l., which is above the tree line where the presence of rocky areas becomes significant. The section of the catchment above 2500 m a.s.l. shows the maximum range in LST, with the highest values on steep south-facing slopes and the lowest values on glaciers and north-facing snow-covered areas. The largest local differences are scattered along the upper crests and can be related to the resolution of the Landsat images, which are too coarse when strong local slope variations occur. The model also shows a strong local overestimation in the main valley floor, on the boundary between sun-lit and shadowed areas. This difference is related to the fact that while Landsat gives an instantaneous snapshot of the scene, the model output is averaged over 1 h, which is the time period of the meteorological data input.

OLS regression results—determinants of LST

The results of OLS regression analyses are shown in Table IV. First, the OLS regression was calculated with LST_G as the dependent variable. Seven independent variables were included at a 1% significance level and one—land cover-type 'settlement'—at a 5% significance level. A highly significant model ($p < 0·001$) was generated with a determination coefficient of 0·847 (adjusted R^2). Second, the OLS regression was calculated with LST_L as the dependent variable. All independent variables were included at a 1% significance level, thereby generating a highly significant model ($p < 0·001$) and a determination coefficient of 0·785 (adjusted R^2). For all variables, no severe multicolinearities were evident.

DOI: 10.1002/eco

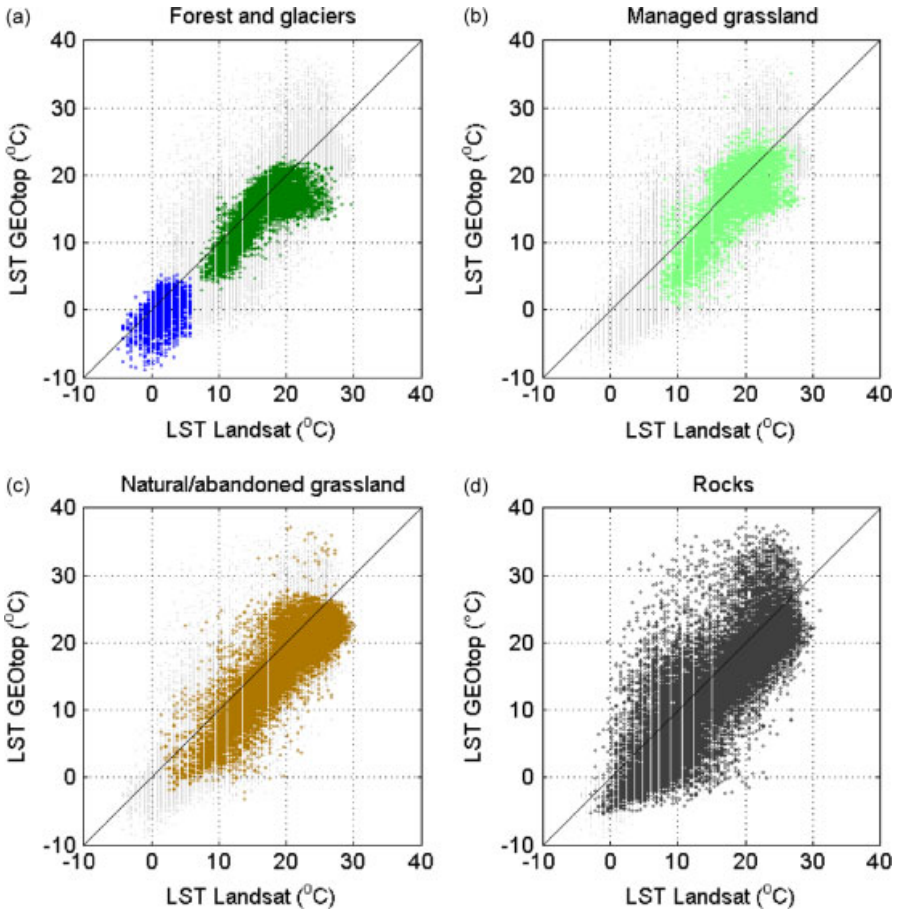

Figure 4. Scatter plot of LST_G versus LST_L (°C), for all pixels (light grey) and for the different land cover classes (highlighted in colour). RMSE for glaciers 2·3 K, forests 2·5 K, managed grassland 4·0 K, natural abandoned grassland 4·2 K and rocks 5·5 K.

Table IV. Results for the OLS regression model with LST_G and LST_L as dependent variables.

	Unstandardized coefficients		Standardized coefficients	Part correlation	T-value (t)	Significance (p-value, two-sided)
	β	SE	β			
Dependent variable = LST_G (model accuracy: adjusted $R^2 = 0.847$)						
Constant	23·646	0·170			139·002	0·000
Sinus of Sun incidence angle Φ	18·446	0·039	0·722	0·694	473·346	0·000
Glaciers	−9·759	0·050	−0·327	−0·284	−193·894	0·000
Elevation Z	−0·005	0·000	−0·351	−0·179	−122·420	0·000
Soil moisture	−18·351	0·259	−0·108	−0·104	−70·764	0·000
Forest	−2·424	0·049	−0·134	−0·072	−49·291	0·000
Managed grassland	−2·344	0·055	−0·095	−0·063	−42·949	0·000
Natural/abandoned grassland	0·363	0·034	0·021	0·016	10·822	0·000
Settlement	−0·312	0·137	−0·004	−0·003	−2·273	0·023
Dependent variable = LST_L (model accuracy: adjusted $R^2 = 0.785$)						
Constant	13·095	0·188			69·580	0·000
Sinus of Sun incidence angle Φ	14·930	0·043	0·626	0·601	346·300	0·000
Glaciers	−12·418	0·056	−0·446	−0·387	−223·024	0·000
Elevation Z	−0·003	0·000	−0·211	−0·108	−62·254	0·000
Natural/abandoned grassland	1·872	0·037	0·113	0·087	50·379	0·000
Forest	−1·544	0·054	−0·091	−0·049	−28·378	0·000
Managed grassland	−0·437	0·060	−0·019	−0·013	−7·238	0·000
Settlement	0·815	0·152	0·010	0·009	5·360	0·000
Soil moisture	1·170	0·287	0·007	0·007	4·078	0·000

The standardized coefficient β is a standardized measure for the influence of each variable on the model. SE is the standard error. The higher the T-value, the greater confidence we have in the coefficient as a predictor (T-values ±2 are acceptable. In the regression models, all input variables exhibit significance and were therefore useful for the prediction of LST_G and LST_L, respectively. The order in the tables follows the relative importance from top to bottom of the independent variables, expressed by the part correlation.

DOI: 10.1002/eco

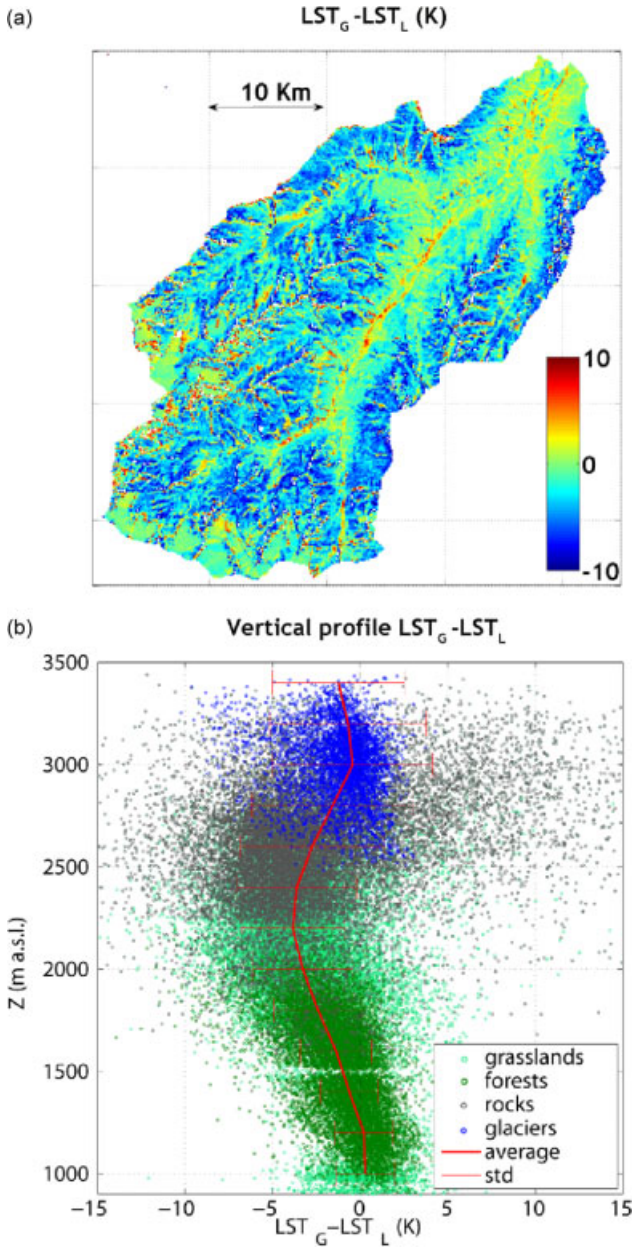

Figure 5. (a) Map of the LST differences between GEOtop and Landsat: LST_G—LST_L (K). (b) LST_G—LST_L as function of the elevation Z. Vegetation, rocks and glaciers are represented with different colours.

Investigation of the scatter plots revealed non-linear dependencies for the variable 'Sinus of Sun incidence angle'. The reason behind this is that on the 'glaciers' land cover-type LST is lower compared with other land cover types for the whole range of Sun incidence angles. However, the requirements of OLS regression were met by including the land cover-type 'glaciers' as a dichotomy variable in our analyses. For all other variables, signs of non-linearity were not evident. Residual analysis confirmed the validity of the model, and the Kolmogorov–Smirnov test revealed no significant deviation from the normal distribution. The standardized residuals' plot revealed no noticeable patterns.

Generally—looking at the part correlations in Table IV—the independent variables 'Sinus of Sun incidence angle', 'glaciers' and 'elevation' revealed the highest influence on both LST_G and LST_L and they explain more than 50% of the LST (quadratic sum of the part correlation was 0·52 in both regression models). While 'Sinus of Sun incidence angle' has a positive correlation—the more perpendicular the sun shines on an area, the higher the LST—'glaciers' and 'elevation Z' are negatively correlated. Areas covered by glaciers as well as higher elevations are characterized by significantly lower LST. The fact that 'glaciers' are identified as the strongest variable among the land cover variables—even stronger than 'elevation'—is justified by its very different temperature regime compared with other land cover types.

For LST_G, following the power of influence in descending order, the other influence factors are: 'soil moisture', 'forest', 'managed grassland', 'natural/abandoned grassland' and 'settlement'. Regarding LST_L, 'soil moisture' was the weakest factor. The stronger influence of 'soil moisture' on LST_G can be explained by the fact that this field is not directly observed, but is a model output.

In summary, the fact that three out of the four most powerfully influential factors match both for LST_G and LST_L corroborates that GEOtop simulates the different processes controlling LST, consistent with the Landsat observations. Although nearly 50% of variance was explained by topographic variables, the influence of land cover was highly significant and nicely reproduced the spatial distribution of LST. 'Forest' was found to be negatively correlated and is a cooling factor. Managed grassland also led to lower LST and natural/abandoned grassland led to increasing LST. This behaviour is consistent with the expected transpiration rates.

In the next section, the effects of (i) Sun incidence angle, (ii) elevation, (iii) land cover and (iv) soil moisture on LST spatial patterns are discussed in detail, with the aid of the simulations 'uniform' and 'wet' indicated in the Simulations Scenarios Section.

Sun incidence angle

One of the major influences on LST in mountain landscapes is the Sun incidence angle $\Phi = \sin(\theta)$, as can be seen immediately in the visual comparison between Figures 3 and 6a. The observed spatial correlation $\rho(LST_L, \Phi)$ is 0·68 and the simulated one $\rho(LST_G, \Phi)$ 0·76 (Table III), while the part correlations coming from the OLS analysis are 0·60 and 0·69 for Landsat and GEOtop, respectively (Table IV). This means that the model is able to correctly simulate the effect of Φ on LST, even if its signature in the model is slightly stronger.

The model permits an understanding of how the dependency of LST on Φ is also affected by the land cover type. As shown in Figure 6b, LST over rocks has the strongest dependency on Φ with respect to the

DOI: 10.1002/eco

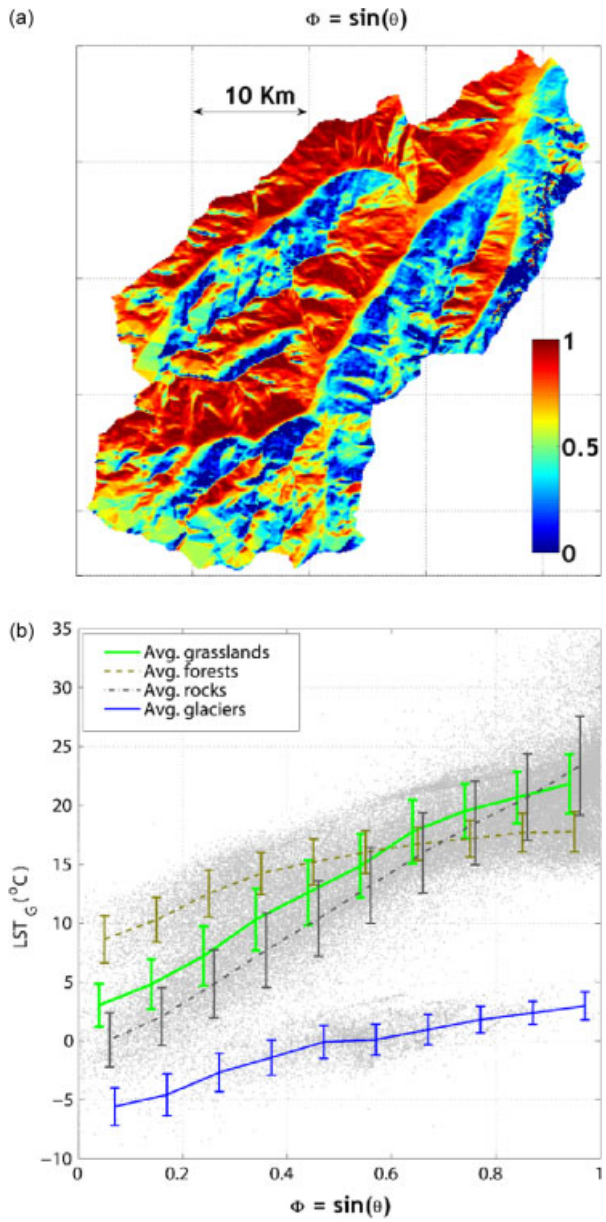

Figure 6. (a) Map of $\Phi = \sin(\theta)$, where θ is the Sun incidence angle at the time of the Landsat overpass. Values of Φ range from 0 (sun at the local horizon) to 1 (sun at local zenith). (b) Modelled LST_G as function of Φ. Each point in the figure represents a pixel. The lines represent the averaged trend with its standard deviation for the different land covers: grasslands, forests, rocks and glaciers.

other land cover types. Forests' LST shows a much weaker dependency on Φ than grasslands', while snow-covered areas show a very different behaviour, with little dependency on Φ. The model assists in an understanding of the physical reason for the weak dependency of LST on Φ in forested areas. The model does not have any parameterization that takes into account different leaves'/crowns' angles, and forests are differentiated from grasslands mostly because of their higher roughness length (Table II), which is an aggregated measure of the intensity of the turbulent heat exchange between leaves and atmosphere. Therefore, model simulations suggest that the canopy structure is the main factor determining the weak dependency of LST on Φ in forest areas.

The output of the simulation 'uniform' highlights the effect of Φ on surface temperature, since a single land cover (grassland) is assumed, and soil moisture is spatially uniform and close to saturation point in the whole basin. In this case, the model shows large local differences, especially in high-elevation regions and glaciers, but the overall spatial correlation $\rho(LST_L, LST_G)$ decreases only from 0·88 to 0·74 (Table III). This test confirms that the Sun incidence angle Φ is a relevant factor when accounting for the LST distribution in a mountain landscape and that an accurate representation of the effects of complex topography is an essential component in ecohydrological models.

Elevation

Another relevant factor which influences LST in mountain environments is the elevation Z. The overall spatial correlation coefficients of the LST fields with Z are $\rho(LST_L, Z) = -0{\cdot}35$ and $\rho(LST_G, Z) = -0{\cdot}51$ (Table III), and the part correlations coming from the OLS analysis are $-0{\cdot}1$ and $-0{\cdot}179$ for Landsat and GEOtop, respectively (Table IV).

Elevation influences LST twofold because air temperature (T_a) tends to decrease with elevation and because land cover tends to be vertically organized. Therefore, we need to analyse the LST_L and LST_G vertical distributions in more detail, and compare them with the T_a vertical profile, in order to discriminate the relative role of T_a with respect to land cover.

Figure 7 helps in an understanding of the role of the T_a vertical profile in determining the vertical distributions of LST_L and LST_G. Three different approximations of the T_a vertical profile are reported in Figure 7: (i) as assumed in the model with a constant lapse rate of -6 K km^{-1} (blue line in Figure 7b); (ii) extrapolated from ground stations at different elevations (black line in Figure 7a) and (iii) from the nearest atmospheric sounding taken at 12 UTM (Munich Airport, Germany; red line in Figure 7a). Both the T_a profiles estimated from sounding and ground stations show a lower lapse rate ($\gamma \approx -2$ K km^{-1}) up to about 1800 m. They then follow a gradient in between the adiabatic wet and dry lapse rate ($\gamma \approx -8$ K km^{-1}).

The comparison of the LST_L vertical distribution with the T_a vertical profile shows that along north-facing slopes, LST_L decreases with elevation, with a gradient similar to the T_a lapse rate, while along south-facing slopes, LST_L shows no dependence on elevation.

Figure 8 helps with an understanding of the roles of land cover and Sun incidence angle Φ in changing the LST vertical distribution. When the only source of spatial variability is topography, as in the case of the 'uniform' simulation (Figure 8b), LST shows a decrease with elevation, both on the north- ($\gamma = -6{\cdot}6$ K km^{-1}) and south-facing ($\gamma = -4{\cdot}7$ K km^{-1}) slopes, with only a slight increase in its variability with elevation. Therefore, it is evident that topography alone is not able to explain the observed LST vertical distribution. Only the inclusion

DOI: 10.1002/eco

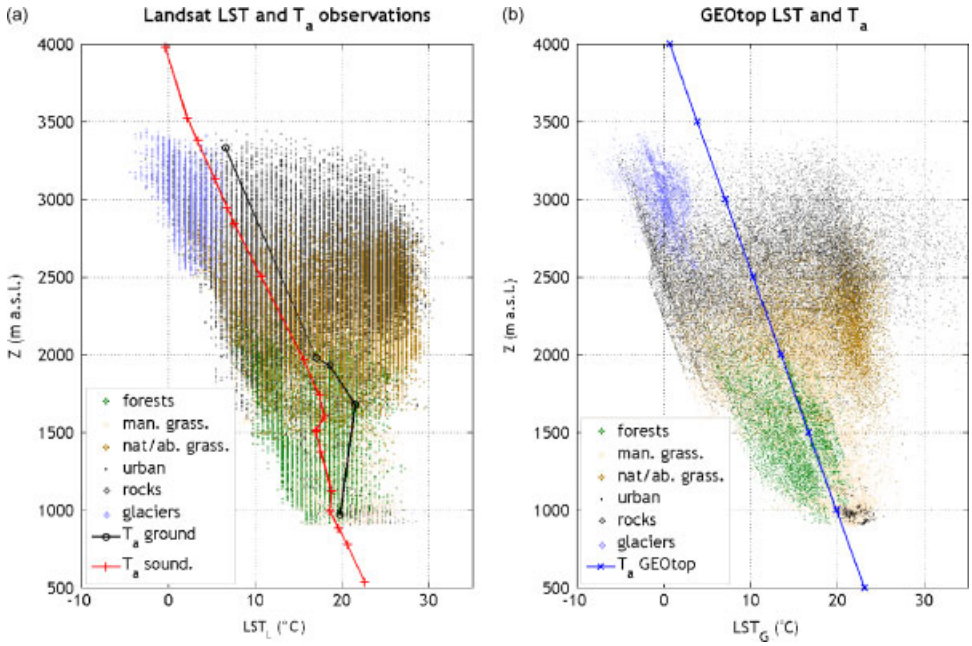

Figure 7. (a) Vertical profile of LST_L (Landsat), with the main land cover classes highlighted with different colours. Black line: 'T_a ground', the vertical profile of T_a, estimated by ground observations. Red line: 'T_a sound', the vertical profile of T_a estimated from the closest available vertical atmospheric sounding at Munich Airport, Germany. (b) Vertical profile of LST_G (GEOtop, simulation 'base'), with the main land cover classes highlighted with different colours. Blue line: 'T_a GEOtop', the vertical profile of T_a assumed in model simulations.

of land cover variability in the model (Figure 8a) permits the reproduction of the observed high LST values on south-exposed slopes at high elevation, covered by rocks or poor alpine grassland associations. Table V supports this observation. In fact, the correlations between LST and elevation $Z\rho(\text{LST}, Z)$ for the northern exposure part ($\Phi < 0{\cdot}5$) of the catchment is much higher than that for the southern exposure part ($\Phi > 0{\cdot}5$). This is true both for Landsat and for the model 'base' simulation. If the land cover is spatially uniform ('uniform' simulation), then the correlation $\rho(\text{LST}, Z)$ is similar for both expositions. This demonstrates the role of land cover variability in controlling LST along southerly exposed slopes.

The main conclusion of this section is that in an alpine catchment, at least for the meteorological conditions analysed in this study (late morning hours during sunny conditions), along north-facing slopes, LST decreases with increasing elevation following T_a. On the contrary, along south-facing slopes, there is no clear LST vertical gradient, because LST is strongly modified by land cover and radiation.

Table V. Correlations $\rho(\text{LST}, Z)$ between LST and elevation Z for all cells, the north-exposed ($\Phi < 0{\cdot}5$) and the south-exposed ($\Phi > 0{\cdot}5$) parts of the catchment.

$\rho(\text{LST}, Z)$	Landsat	Simulation base	Simulation uniform
All cells	−0·35	−0·38	−0·51
North	−0·57	−0·67	−0·67
South	0·01	−0·07	−0·80

Land cover

We now analyse in detail the effect of land cover on LST. Figure 9 shows the distribution frequency for the main land cover classes of LST_L and LST_G and the corresponding distribution of the elevation Z and Φ. It highlights the interplay between climatic, topographic and human factors in controlling land cover distribution in an alpine catchment (Tappeiner *et al.*, 2008).

Glaciated or snow-covered areas (Figure 9a) show a sharp LST distribution around 0 °C. Rocky regions show the maximum dispersion (Figure 9d). Natural/abandoned grassland represents a kind of transition class from the richest (high LAI) managed grasslands to the pure rocky areas. The LST_L distribution of natural/abandoned grassland has a similar spread as the rock class (Figure 9d), but with a peak shifted for higher values (Figure 9g). This is related to two factors: first, high-altitude natural grasslands, being temperature limited, naturally tend to grow more along south-facing slopes (Körner and Paulsen, 2004), as appears from the Φ distribution in Figure 9k. Second, dwarf alpine vegetation tend to warm up more quickly than taller, lower altitude vegetation (Grace *et al.*, 1989), as will be discussed later. Richer vegetation, such as managed grasslands, exerts a dampening effect on LST_L (Figure 9i), because vegetation has a stronger aerodynamic coupling and higher evapotranspiration rates with respect to rocky or bare soil locations. Forests (Figure 9m) show lower LST compared to grasslands because of the stronger aerodynamic coupling of taller vegetation (Wilson *et al.*, 1987). Their LST distribution presents two peaks because forests are mainly located on steep side slopes, either north or south facing.

DOI: 10.1002/eco

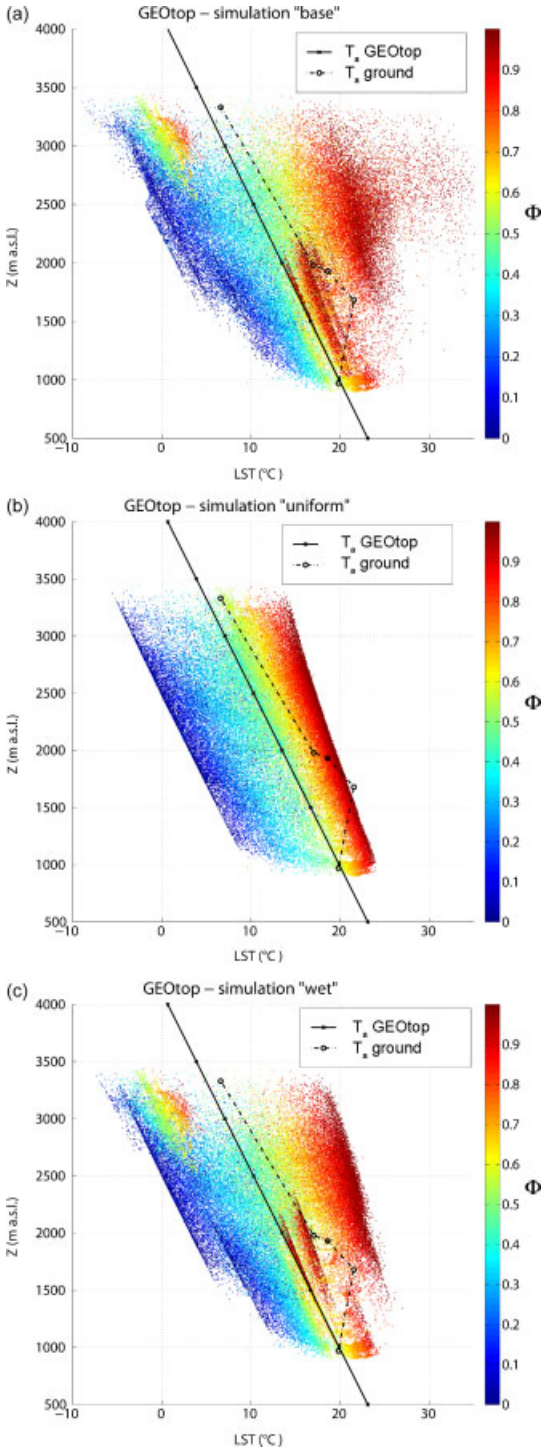

Figure 8. (a) Vertical profile of LST_G for the 'base' simulation, which considers a realistic land cover distribution, with the corresponding Sun incidence angle $\Phi = \sin(\theta)$ highlighted in colours (blue indicates $\Phi = 0$; red indicates $\Phi = 1$). (b) Vertical profile of LST_G for the 'uniform' simulation, where a uniform land cover is assumed. (c) Vertical profile of LST_G for the 'wet' simulation. Continuous line: 'T_a GEOtop', vertical profile of T_a assumed in model simulations. Dotted line: 'T_a ground', vertical profile of T_a, estimated by ground observations.

The effects of alpine vegetation on LST distribution

The different thermal and structural properties of alpine vegetation change the microclimate close to the soil surface and, as we have seen before, the LST altitudinal gradient (Körner, 2003). In particular, prostrate vegetation (included here in the land cover class 'natural/abandoned grassland'), frequent in high-altitude alpine rocky habitats, creates its own microclimate decoupled from air temperature (Cernusca, 1976). Cushion plants and low-stature dense shrubs work as a particularly efficient heat trap and have higher LST—T_a compared with taller plants such as trees, which protrude through the shrub layer and operate close to air temperature most of the time (Körner *et al.*, 2003). Cernusca and Seeber (1989a,b) found no trend with elevation in canopy surface temperature along a south-exposed transect ranging from 1612 to 2300 m a.s.l. which included a hay meadow, an alpine pasture and two grass heath communities. In addition, they found an increase in LST—T_a difference from 10 K up to more than 25 K with altitude.

We now want to verify whether the remote sensing image considered shows the same trend that has been observed—to our knowledge—only at the plot scale, by directly measuring leaf temperature or using ground-based thermographic imagery (Körner, 2007). In fact, our results show that the maximum LST_L—T_a difference increases with elevation from about 8 K at 1000 m up to around 20 K at 2500 m (Figure 7).

In Figure 10, the frequency histogram of LST_L for the main land cover types is separated between north- ($\Phi < 0{\cdot}5$) and south-facing ($\Phi > 0{\cdot}5$) slopes, in order to minimize the effect of exposure and isolate the thermal behaviour of the different vegetation types. Figure 10 clearly shows how natural grasslands tend to increase LST on south-facing slopes much more than other land cover types. The peak of the LST distribution is 12 K warmer on south-facing slopes over natural grasslands, while is only 4 K warmer for forests. Model simulations show a similar LST difference. Therefore, the present analysis highlights the capacity of alpine vegetation to change the microclimate close to the surface. Results show how this process has an impact not only at the plot scale, but also at the landscape scale, and that it can also be detected at relatively coarse resolution (60 m) satellite images. The landscape scale impact of this process may also have implications on climate at the regional scale (Bertoldi *et al.*, 2008).

Role of soil moisture spatial variability

The thermal behaviour of different land covers can be related to their surface and structural properties, which control the efficiency of both ground and atmospheric heat transfer, or can be controlled by energy partitioning between sensible and latent heat flux. Soil moisture influences sensible and latent heat partitioning and therefore LST. However, for the humid climate considered in this study, the impact of soil moisture spatial variability on LST is quite limited at the catchment scale. In fact, the 'base' simulation, with spatially variable soil moisture conditions, and the 'wet' simulation, with uniformly saturated soil, show a similar conformity with the observed LST_L (Table III). The OLS analysis confirms the weak role of soil moisture (Table IV). However,

DOI: 10.1002/eco

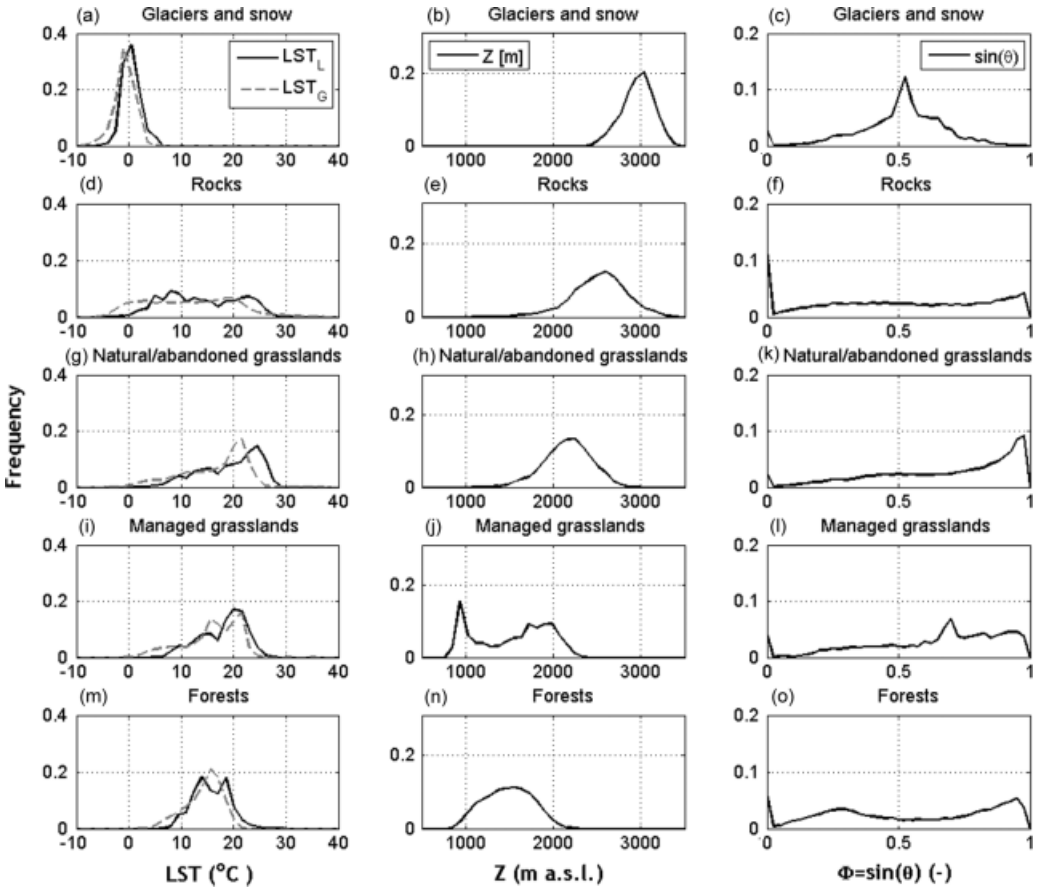

Figure 9. Frequency distribution of LST_L (black line), LST_G (dotted grey line), elevation Z and $\Phi = \sin(\theta)$, where θ is the Sun incidence angle, for the main land cover classes: glaciers and snow (a, b, and c), rocks (d, e and f), natural/abandoned grassland (g, h and k), managed grassland (i, j and l) and forest (m, n and o).

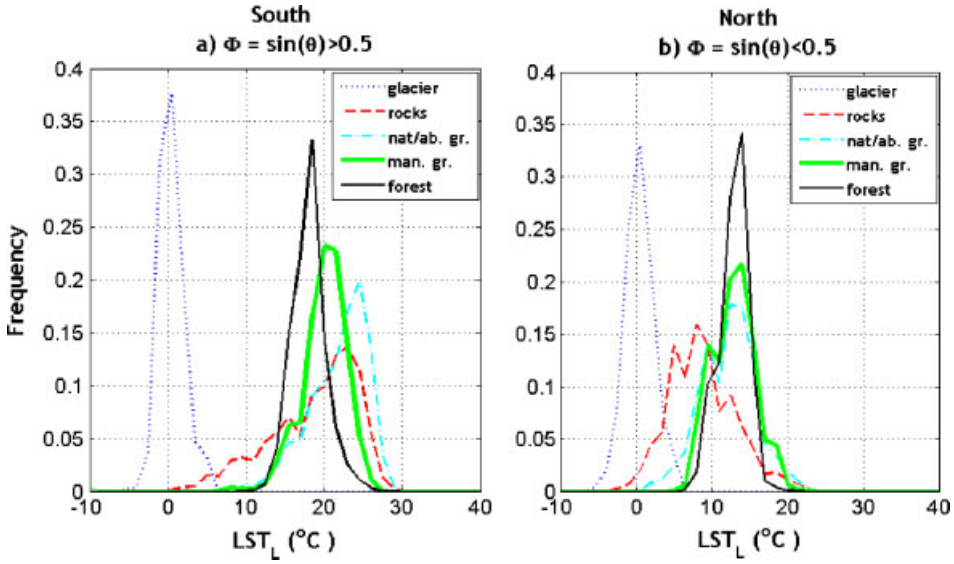

Figure 10. Frequency distribution of LST_L, for the main land cover classes; (a) only the south-exposed cells ($\Phi > 0{\cdot}5$) are considered; (b) only the north-exposed cells ($\Phi < 0{\cdot}5$) are considered.

simulation results suggest that locally, in high-elevation regions where evaporation from shallow soil is dominant, the observed high LST values can be related to limited evaporation of soil moisture from shallow soil. In fact, the comparison of the results for the simulations 'base' and 'wet' in Figure 8a and c suggests that the effect of soil moisture spatial variability is the introduction of a relevant scatter in the simulated LST for pixels along south-exposed mountain ridges and rocky or sparsely vegetated high-elevation locations. This scatter alters the LST vertical gradient and is also evident in the Landsat data (Figure 7a).

DOI: 10.1002/eco

In the vegetated lower part of the catchment, soil moisture does not show any relevant effect on LST. This is because the vegetation is not under water stress conditions and the strong differences in LST observed in the different vegetation classes are more related to differences in the structural properties of the vegetation (i.e. z_0) than to differences in the transpiration rate. This behaviour has also been verified by the experimental studies of Cernusca and Seeber (1989a,b), who found that, in a catchment with a similar climate in the Austrian Alps, vegetation was never under stress conditions throughout the whole year, and evapotranspiration was best estimated by the Priestley and Taylor (1972) model assuming no water limitation.

CONCLUSIONS

In this study, the spatial distribution of LST in an alpine catchment, the Stubai Valley in Austria, observed by a Landsat image and simulated by the GEOtop ecohydrological model, has been compared and analysed. The GEOtop model is able to reproduce the spatial patterns of the LST distribution estimated from remote sensing, with a correlation coefficient of 0·88 and with minimal calibration of the model parameters. The model has been used as a tool to separate the different environmental factors controlling LST in mountain regions through a series of virtual experiments (Dunn *et al*., 2008) and it has been able to represent the specific sensitivity of LST on elevation, land cover, solar radiation and soil moisture in a complex mountain environment.

Considering the time of day and atmospheric conditions in this study, the major factors controlling the LST spatial distribution were incoming solar radiation and land cover variability. The results revealed that land cover strongly modified LST on south-facing slopes, while on north-facing slopes, LST appeared to follow the air temperature elevational gradient more closely. In particular, the strong differences in LST observed in the different vegetation classes were mainly related to differences in the vegetations' structural properties rather than differences in transpiration rate. For the humid climate considered in this study, moisture distribution exerted only a minor influence on LST, except along mountain ridges and south-exposed steep slopes.

Therefore, results indicate that key features to be implemented in a distributed hydrological model in order to properly simulate LST in mountain environments are the capacity to explicitly simulate the effects of complex topography on the surface energy exchange processes and an accurate representation of land cover types, particularly those of canopy properties, which control the efficiency of the turbulent energy exchanges (i.e. z_0).

The analysis indicates that the use of remote sensing information can be helpful in assessing the capacity of ecohydrological models to represent the high spatial pattern variability of mountainous areas and the related surface energy exchange processes (Schulz *et al*., 2006). This fine-scale heterogeneity has an impact on large-scale fluxes and therefore on catchment-scale water and energy budgets when the processes involved are not linear (Raupach and Finnigan, 1995). The scaling issue is a key factor in order to have the correct representation of processes in hydrological modelling (McCabe and Wood, 2006).

While this study refers to a single LST image, the proposed approach can be extended to other climatic and environmental conditions, in order to improve the capacity of modelling the effects of topography, soil moisture and land cover on the spatial distribution of LST in complex mountain environments. Future stages of the work intend to take into consideration other information coming from remote sensing analysis such as LAI and albedo maps.

ACKNOWLEDGEMENTS

This work was partially funded by the Provincia Autonoma di Bolzano research grant: 'Climate Change in South Tyrol'. We thank Dr G. Wohlfahrt and Dr E. Tasser for their useful suggestions and the data they provided. We also thank Dr G. Tappeiner for his help with the statistical analyses and the two anonymous referees for their critical and thoughtful comments.

REFERENCES

Becker A, Körner C, Brun JJ, Guisan A, Tappeiner U. 2007. Ecological and land use studies along elevational gradients. *Mountain Research and Development* **27**(1): 58–65.

Bertoldi G, Kustas WP, Albertson JD. 2008. Estimating spatial variability in atmospheric properties over remotely sensed land-surface conditions. *Journal of Applied Meteorology and Climatology* **47**: 2147–2165. DOI: 10.1175/2007JAMC1828.1.

Bertoldi G, Rigon R, Over T. 2006. Impact of watershed geomorphic characteristics on the energy and water budgets. *Journal of Hydrometeorology* **7**: 389–403.

Best MJ. 1998. A model to predict surface temperatures. *Boundary-Layer Meteorology* **88**(2): 279–306.

Beven KJ, Freer J. 2001. A dynamic TOPMODEL. *Hydrological Processes* **15**: 1993–2011.

Brooks PD, Vivoni ER. 2008. Mountain ecohydrology: quantifying the role of vegetation in the water balance of montane catchments. *Ecohydrology* **1**: 187–192. DOI: 10.1002/eco.27.

Cernusca A. 1976. Bestandesstruktur, Bioklima und Energiehaushalt von alpinen Zwergstrauchbeständen. *Oecologia Plantarum* **11**: 71–102.

Cernusca A, Seeber MC. 1989a. Phytomasse, Bestandesstruktur and Mikroklima von Grasland-Ökoystemen zwischen 1612 und 2300 m in den Alpen. In *Struktur und Funktion von Grasland ökosystemen im Nationalpark Hohe Tauern*, vol. 13, *Veröffentlichen*, Cernusca A (ed). Österreichischen MaB-Programs, Österreichische Akademie der Wissenshaften, Universitätsverlag Wagner: Innsbruck; 420–461.

Cernusca A, Seeber MC. 1989b. Energiehaushalt einer Mähwiese (1612 M MH), einer Almweide (1921 M MH) und einer Alpinen Grasheide (2300 M MH) in den Österreichischen Zentralapen. In *Struktur und Funktion von Graslandökosystemen im Nationalpark Hohe Tauern*, vol. 13, *Veröffentlichen*, Cernusca A. (ed). Österreichischen MaB-Programs, Österreichische Akademie der Wissenshaften, Universitätsverlag Wagner: Innsbruck; 462–495.

Cernusca A, Tappeiner U, Bayfield N. 1999. *ECOMONT—Ecological Effects of Land-Use Changes in Mountain Areas of Europe*. Blackwell Wissenschaftsverlag: Berlin.

Chow FK, Weigel AP, Street RL, Rotach MW, Xue M. 2006. High-resolution large-eddy simulations of flow in a steep alpine valley. Part I: methodology, verification, and sensitivity experiments. *Journal of Applied Meteorology and Climatology* **45**: 63–86.

Diak GR, Mecikalski JR, Anderson MC, Norman JM, Kustas W, Torn RD, DeWolf RL. 2004. Estimating land-surface energy budgets from space: review and current efforts at the University of Wisconsin-Madison and USDA-ARS. *Bulletin of the American Meteorological Society* **1**: 65–78.

Dickinson RE, Heanderson-Sellers A, Rosenzweig C, Sellers PJ. 1991. Evapotranspiration models with canopy resistance for use in climate models, a review. *Agricultural and Forest Meteorology* **54**: 373–388.

Dubayah A, Dozier J, Davis FW. 1990. Topographic distribution of clear-sky radiation over the Konza Prairie, Kansas. *Water Resources Research* **26**(4): 679–690.

Dunn SM, Freer J, Weiler M, Kirkby HJ, Seibert J, Quinn PF, Lischeid G, Tetzlaff D, Soulsby C. 2008. Conceptualization in catchment modelling: simply learning? *Hydrological Processes* **22**: 2389–2393.

Endrizzi S. 2009. *Snow Cover Modelling at a Local and Distributed Scale Over Complex Terrain*, 15th edn. *Monographs of the Doctoral School in Environmental Engineering*. Department of Civil and Environmental Engineering. Universitá degli Studi di Trento: Italy.

Erbs DG, Klein SA, Duffie JA. 1982. Estimation of the diffuse radiation fraction for hourly, daily and monthly average global radiation. *Solar Energy* **28**(4): 293–304.

Findell K, Shevliakova E, Milly P, Stouffer R. 2007. Modeled impact of anthropogenic land cover change on climate. *Journal of Climate* **20**: 3621–3634.

Garen DC, Marks D. 2005. Spatially distributed energy balance snowmelt modelling in a mountainous river basin: estimation of meteorological inputs and verification of model results. *Journal of Hydrology* **315**: 126–153.

Grace J, Allen SJ, Wilson C. 1989. Climate and the meristem temperatures of plant-communities near the tree-line. *Oecologia* **79**(2): 198–204.

Grayson R, Blöschl G. 2000. *Spatial Patterns in Catchment Hydrology, Observations and Modelling*. Cambridge University Press: Cambridge.

Hammerle A, Haslwanter A, Tappeiner U, Cernusca A, Wohlfahrt G. 2008. Leaf area controls on energy partitioning of a temperate mountain grassland. *Biogeosciences* **5**: 421–431.

Heimsath MA, Dietrich WE, Nishiizumi K, Finkel R. 1997. The soil production function and landscape equilibrium. *Nature* **388**: 358–361.

Iqbal M. 1983. *An Introduction to Solar Radiation*. Academic Press: Orlando, FL.

Ivanov VY, Vivoni ER, Bras RL, Entekhabi D. 2004. Preserving high-resolution surface and rainfall data in operational-scale basin hydrology: a fully-distributed physically-based approach. *Journal of Hydrology* **298**: 80–111.

Kitanidis PK. 1997. *Introduction to Geostatistic Application in Hydrogeology*. Cambridge University Press: Cambridge.

Körner C. 2003. *Alpine Plant Life*, 2nd edn. Springer: Heidelberg.

Körner C. 2007. Climatic treelines: conventions, global patterns, causes. *Erdkunde* **61**: 316–324.

Körner C, Paulsen J. 2004. A world-wide study of high altitude treeline temperatures. *Journal of Biogeography* **31**(5): 713–732.

Körner C, Paulsen J, Pelaz-Riedl S. 2003. A bioclimatic characterization of Europe's alpine areas. In *Alpine Biodiversity in Europe*, vol. 167, *Ecological Studies*, Nagy L, Grabherr G, Körner C, Tompson D. (eds). Springer: Berlin; 13–28.

Kunstmann H, Stadler C. 2005. High resolution distributed atmospheric—hydrological modelling for alpine catchments. *Journal of Hydrology* **314**: 105–124.

Larcher W. 2003. *Physiological Plant Ecology*, 4th edn. Springer-Verlag: New York.

Lawford R, Stewart R, Roads J, Isemer H-J, Manton M, Marengo J, Yasunari T, Benedict S, Koike T, Williams S. 2004. Advancing global and continental scale hydrometeorology: contributions of the GEWEX Hydrometeorology Panel (GHP). *Bulletin of the American Meteorological Society.* **85**(12): 1917–1930.

Li F, Jackson TJ, Kustas WP, Schmugge TJ, French AN, Cosh M, Bindlish R. 2004. Deriving land surface temperature from landsat 5 and 7 during SMEX02/SMACEX. *Remote Sensing of Environment* **92**: 521–534.

McCabe M, Wood EF. 2006. Scale influences on the remote estimation of evapotranspiration using multiple satellite sensors. *Remote Sensing of Environment* **105**: 271–285.

McNaughton KG, Jarvis PG. 1991. Effects of spatial scale on stomatal control of transpiration. *Agricultural and Forest Meteorology* **54**: 279–301.

Monin AS, Obukhov AM. 1954. Basic laws of turbulent mixing in the atmosphere near the ground. *Trudy Geofizicheskogo Instituta, Akademiya Nauk SSSR* **24**(151): 1963–1987.

Norman JM, Kustas WP, Humes KS. 1995. A two-source approach for estimating soil and vegetation energy fluxes from observations of directional radiometric surface temperature. *Agricultural and Forest Meteorology* **77**: 263–293.

Pomeroy JW, Toth B, Granger RJ, Hedstrom NR, Essery RLH. 2003. Variation in surface energetics during snowmelt in a subarctic mountain catchment. *Journal of Hydrometeorology* **4**: 702–719.

Priestley CHB, Taylor RJ. 1972. On the assessment of surface heat flux and evaporation using large-scale parameters. *Monthly Weather Review* **100**: 81–92.

Qin Z, Karnieli A, Berliner P. 2001. A mono-window algorithm for retrieving land surface temeprature from landsat TM and its application to the Israel–Egypt border region. *International Journal of Remote Sensing* **18**: 3719–3746.

Rampanelli G. 2004. *Investigation of diurnal atmospheric boundary layer dynamics in alpine valleys*. PhD Dissertation in Environmental Engineering, University of Trento: Italy.

Raupach MR, Finnigan JJ. 1995. Scale issues in boundary-layer meteorology: surface energy balance in heterogeneous terrain. *Hydrological Processes* **9**: 589–612.

Rigon R, Bertoldi G, Over TM. 2006. GEOtop: a distributed hydrological model with coupled water and energy budgets. *Journal of Hydrometeorology* **7**: 371–388.

Romano N, Palladino M. 2002. Prediction of soil water retention using soil physical data and terrain attributes. *Journal of Hydrology* **265**: 56–75.

Schulz K, Seppelt R, Zehe E, Vogel HJ, Attinger S. 2006. Importance of spatial structure in advancing hydrological sciences. *Water Resources Research* **42**(3): W03S03. DOI: 10.1029/2005WR004301.

Simoni S, Zanotti F, Bertoldi G, Rigon R. 2007. Modelling the probability of occurrence of shallow landslides and channelized debris flows using GEOtop-FS. *Hydrological Processes* **22**(4): 532–545. DOI: 10.1002/hyp.6886.

Stull RB. 1988. *An Introduction to Boundary Layer Meteorology*. Kluwer Academic Publisher: Boston.

Tappeiner U, Tasser E, Leitinger G, Tappeiner ACG. 2008. Effects of historical and likely future scenarios of land use on above and belowground vegetation carbon stocks of an alpine valley. *Ecosystems* **11**: 1383–1400. DOI: 10.1007/s10021-008-9195-3.

Tasser E, Ruffini F, Tappeiner U. 2009. A integrative approach for analysing landscape dynamics in diverse cultivated and natural mountain areas. *Landscape Ecology* **24**: 611–628. DOI: 10.1007/s10980-009-9337-9.

Tenhunen J, Geyer R, Adiku S, Reichstein M, Tappeiner U, Bahn M, Cernusca A, Dinh NQ, Kolcun O, Lohila A, Otieno D, Schmidt M, Wang Q, Wartinger M, Wohlfahrt G. 2009. Influences of changing land use and CO_2 concentration on ecosystem and landscape level carbon and water balances in mountainous terrain of the Stubai Valley, Austria. *Global and Planetary Change* **67**(1-2): 29–43.

Thome K, Whittington E, LaMarr J, Anderson N, Nandy P. 2000. Early ground-reference calibration results for Landsat-7 ETMC using small test sites. In Algorithms for Multispectral, Hyperspectral, and Ultraspectral Imagery VI, edited by Sylvia S. Shen; Michael R. Descour, Proc. Of SPIE. **4049**: 134–142. DOI: 10.1117/12.410334.

Turner MG, Gardner RH, O'Neill RV. 2001. *Landscape Ecology in Theory and Practice: Pattern and Process*. Springer: New York.

Vereecken H, Maes J, Feyen J, Darius P. 1989. Estimating the soil moisture retention characteristic from texture, bulk density and carbon content. *Soil Science* **148**: 389–403.

Wang L, Koikea T, Yang K, Yeh PJ. 2009. Assessment of a distributed biosphere hydrological model against MODIS land surface temperature and its application in the upper Tone river basin. *Journal of Hydrology* **377**: 21–34.

Weigel AP, Chow FK, Rotach MW. 2007. The effect of mountainous topography on moisture exchange between the "surface" and the free atmosphere. *Boundary-Layer Meteorology* **125**: 227–244. DOI: 10.1007/s10546-006-9120-2.

Wigmosta MS, Vail L, Lettenmaier D. 1994. A distributed hydrology-vegetation model for complex terrain. *Water Resources Research* **30**(6): 1665–1679.

Wilson C, Grace J, Allen S, Slack F. 1987. Temperature and stature: a study of temperatures in montane vegetation. *Functional Ecology* **1**(4): 405–413.

Wohlfahrt G, Bahn M, Newesely CH, Sapinsky S, Tappeiner U, Cernusca A. 2003. Canopy structure versus physiology effects on net photosynthesis of mountain grasslands differing in land use. *Ecological Modelling* **170**: 407–426.

Zanotti F, Endrizzi S, Bertoldi G, Rigon R. 2004. The GEOtop snow module. *Hydrological Processes* **18**: 3667–3679. DOI:10.1002/hyp.5794.